CHEMISTRY OF MATERIALS

Article

pubs.acs.org/cm

Hierarchically Structure-Directing Effect of Multi-Ammonium Surfactants for the Generation of MFI Zeolite Nanosheets

Woojin Park,[†,‡] Doae Yu,[†] Kyungsu Na,[†,‡] Kim E. Jelfs,[§] Ben Slater,[⊥] Yasuhiro Sakamoto,[∥] and Ryong Ryoo*[,†,‡]

[†]Center for Functional Nanomaterials, Department of Chemistry, KAIST, Daejeon 305-701, Korea

[‡]Graduate School of Nanoscience and Technology (WCU), KAIST, Daejeon 305-701, Korea

[§]Department of Chemistry and Center for Materials Discovery, University of Liverpool, Crown Street, Liverpool, U.K.

[⊥]Department of Chemistry, University College London, 20 Gordon Street, London WC1H 0AJ, U.K.

[∥]Nanoscience and Nanotechnology Research Center, Osaka Prefecture University, Sakai 599-8570, Japan

Supporting Information

ABSTRACT: Multi-quaternary ammonium surfactants can assemble co-operatively with silicate anions to generate MFI zeolite nanosheets, where the ammonium acts as a structure-directing agent for the microporous zeolite, while the surfactant tails assemble into a lamellar micelle. The two-level structure-directing effects have been investigated for various molecules with the formula of *tail*-$N^+(CH_3)_2$–{*spacer*–N^+R_2}$_{n-1}$–*R**. Here, *n* is varied over 1–4. The *tail* is selected among linear alkyl chains (C_mH_{2m+1}, *m* = 6–22). The *spacer* is an alkylene bridge (–C_iH_{2i}–, *i* = 3, 6 and 8). *R* and *R** are alkyl groups (C_jH_{2j+1}, *j* = 1–6). The result highlights that the surfactant molecule should be equipped with at least 2 suitable ammonium groups for the formation of zeolite structure, in addition to the amphiphilic nature and micelle packing ability. Moreover, the thickness of the nanosheets can be increased and tailored according to the number of the ammonium groups. Detailed consideration of the effects of template molecular features may be useful for the design of hierarchically structure-directing surfactants for nanomorphic zeolites.

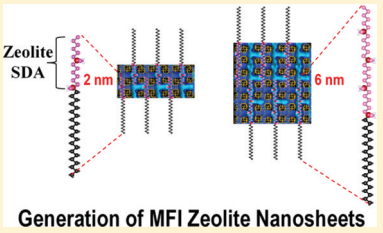

KEYWORDS: *structure directing agent, organic surfactant, single unit cell thickness, MFI zeolite nanosheet, unilamellar, multilamellar, hierarchical zeolite, nanomorphic zeolite, mesoporous zeolite, mesoporous silica*

INTRODUCTION

Zeolites are crystalline microporous aluminosilicate materials, which are widely used as molecular shape-selective catalysts and adsorbents owing to the regular pore arrangement with uniform diameters.[1−3] Some zeolites occur naturally as mineral rocks, formed in volcanic regions under hydrothermal conditions. For industrial applications, zeolites are synthesized according to procedures using inorganic cations or organic ammonium species as structure-directing agents (SDAs). The SDAs lead to specific zeolite structures through their cooperative assembly with polymerizing silicates under hydrothermal synthesis conditions. Thus, zeolites are crystallized as incorporated SDA molecules within the aluminosilicate framework.[1,2,4,5] The nanospace occupied by the organic SDA is converted to a pore or channel after the SDA removal by combustion in air, at high temperature. The pore apertures are normally less than 1 nm, often causing serious diffusion limitations in applications.[3,6,7]

Mesoporous silica and aluminosilicate materials can be synthesized by using surfactant micelles as the pore-generating agents (porogens).[8−10] These materials have much larger pores than zeolite micropores (typically, pore diameters in the range of 2–50 nm). The mesopores are very uniform, and moreover, the diameters can be precisely tailored by the size of the surfactant molecules. These characteristics are very useful to resolve the diffusion limitations in catalysis and adsorption of bulky molecules. However, the mesopore walls in ordinary mesoporous silica and aluminosilicate materials, such as MCM-41[9] and SBA-15,[10] are built with noncrystalline frameworks. The noncrystalline nature is a critical factor that prevents the framework acidity from rising to a level that would be practicable for various catalytic applications.[11,12] From the point of view of the catalytic applications, it is highly desirable to have mesoporous architectures that are built with zeolite-like, microporous crystallinity, instead of the noncrystalline frameworks of the aforementioned mesoporous materials. The mesopores in such crystalline materials are suitable for adsorption of bulky molecules. The zeolitic frameworks with strong acidity are very effective for the acid catalytic function.[13,14] In addition, the small zeolitic micropores within the mesopore walls can be used as catalytic nanoreactors for small molecular transformation.[15] The hierarchically mesoporous-microporous structure (or hierarchical structure) has the advantage of facile diffusion to micropores via the mesopores. Hence, there were numerous reports in recent years aiming at synthesizing mesoporous aluminosilicate materials with zeolite-

Received: June 16, 2011
Revised: October 18, 2011
Published: November 8, 2011

like frameworks.[16−23] For example, zeolites were synthesized in the form of nanocrystals, so that the intercrystalline void space became mesoporous channels.[16] Bulk zeolite crystals were partially dissolved with an acid[17] or base[18,19] to generate intracrystalline mesopores. Pre-made nanoparticles,[20] nanotubes,[21] nanoporous materials[22] were used as templates to synthesize a zeolite containing mesopores. Organosilane-type surfactants were added as a mesopore-generating agent in zeolite synthesis, too.[23]

Recently, Choi et al. tried an organic surfactant with the formula of $C_{22}H_{45}-N^+(CH_3)_2-C_6H_{12}-N^+(CH_3)_2-C_6H_{13}$ (hereafter, $C_{22-6}N_2$) as a SDA for MFI zeolite,[24] instead of the typically used tetrapropylammonium (TPA^+). The experiment resulted in the formation of MFI zeolite nanosheets about 2 nm thick, which corresponded to only a single unit-cell dimension along the *b*-axis. The formation of the zeolite nanosheets indicates that the diquaternary ammonium headgroup in the surfactant served as the MFI zeolite SDA while the C_{22} alkyl tails were intermolecularly assembled to direct the lamellar-type nanosheet. Use of a surfactant containing a zeolite SDA like $C_{22-6}N_2$ is quite attractive as an approach for the synthesis of hierarchical zeolite, particularly, in view of mesopore uniformity and controllability. However, the zeolite synthesis using such hierarchical structure-directing surfactants is thus far limited to the lamellar mesostructure.[24−26] Before targeting other hierarchical zeolites, it is necessary to investigate the detailed structural effects of the surfactant molecules for zeolite structure generation.

In this work, we have investigated the structure-directing ability of multi-quaternary ammonium surfactants with various structures for the generation of MFI zeolite nanosheets. The surfactants were prepared by joining quaternary ammonium groups in series to an alkyl tail as in $C_{22}H_{45}-N^+(CH_3)_2-[C_6H_{12}-N^+(CH_3)_2]_{n-1}-C_6H_{13}$, where *n* was varied from 1 to 4. The spacers between ammonium groups were varied with $-C_3H_6-$, $-C_6H_{12}-$, and $-C_8H_{16}-$. The methyl groups at the terminal ammonium were replaced with ethyl, propyl, and butyl. In addition, the tail length was varied over the range of C_6-C_{22} alkyl chains. These molecules were tested as supramolecular SDAs in the synthesis of siliceous MFI zeolite nanosheets under hydrothermal conditions. The silica products thus obtained were characterized by powder X-ray diffraction (XRD), N_2 adsorption, high-resolution scanning electron microscopy (SEM), and transmission electron microscopy (TEM). The zeolite synthesis result using these surfactants is reported in the present article for a deeper understanding about the detailed structural effects of the multi-ammonium surfactants for directing zeolite structures.

EXPERIMENTAL SECTION

Preparation of Surfactants. The quaternary ammonium surfactants used in this work are listed in Table 1. These surfactants were synthesized and purified in the laboratory via alkylation of amines, similar to previous works.[24,25] Purities were confirmed by ^{1}H NMR. Detailed procedures are given in Supporting Information.

Zeolite Synthesis. The quaternary-ammonium surfactants in Table 1 were used as zeolite SDAs as synthesized in the bromide form, or used after the counterion Br^- was replaced with OH^- by stirring with an anion-exchange resin (MTO-Dowex SBR LCNG OH form, Supelco) in a flask. The silica source was water glass (aqueous solution of sodium silicate, 29 wt % SiO_2, Si/Na = 1.75) received from Shinheung Silicate or tetraethylorthosilicate (TEOS, 95%) purchased from Junsei. Hydrothermal synthesis of zeolite was performed at the gel compositions given in Table 2. In a typical synthesis with $C_{22-6}N_n$ (n = 2, 3, or 4), 4.17 g (0.0200 mol) of TEOS was added into 14.4 g (0.800 mol) of water containing surfactant under vigorous stirring to give the gel composition of 100 SiO_2: *a* $C_{22-6}N_n(OH)_n$: 3800 H_2O: 400 EtOH, where *a* was varied between 5 and 2.5 to fix the ratio of SiO_2/N^+ at 10. The $C_{22-6}N_2$ surfactant was used in the hydroxide form as dissolved in distilled water, and 400 EtOH was automatically generated because of hydrolysis of 100 TEOS. 4000 H_2O was used to obtain the gel composition, among which 200 H_2O was consumed for the hydrolysis of 100 TEOS. However, synthesis conditions were not so sensitive to such a slight change in water content, as we demonstrated in a recent report.[26] After continuous mixing for 6 h at 60 °C, the resultant gel was transferred into a Teflon-lined stainless-steel autoclave. The autoclave was tumbled vertically at 60 rpm in an oven heated at 140 °C for a desired period (<10 d). The zeolite product was collected by filtration, dried at 100 °C, and calcined in air at 550 °C. Zeolite synthesis experiments with other surfactants were carried out in the same manner by referring to the literatures,[25,26] except for the differences in the gel composition, silica source, and reaction time as in Table 2.

Table 1. Quaternary Ammoniums Tested as Zeolite SDA

SDA Structure	Notation
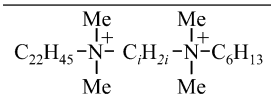	$C_{22-i}N_2$ i = 3, 6, 8
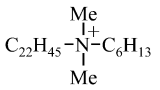	$C_{22}N_1$
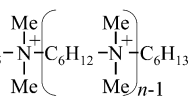	$C_{22-6}N_n$ n = 2, 3, 4
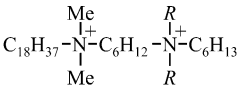	$C_{18-6}N_2(R_2)$ R: Me = CH_3, Et = C_2H_5, Pr = n−C_3H_7, Bu = n−C_4H_9
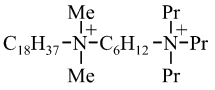	$C_{18-6}N_2(Pr_3)$
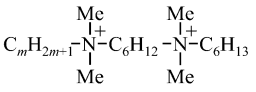	$C_{m-6}N_2$ m = 6, 8, 10, 12

Materials Characterization. All organic molecules synthesized here were identified by solution ^{1}H NMR (Bruker Avance instrument 300 MHz). XRD patterns were obtained with a Rigaku Multiflex diffractometer using Cu Kα radiation (λ = 0.1541 nm) at 30 kV, 40 mA (1.2 kW). High-resolution SEM images were taken with a Hitachi S-4800 (2.0 kV, in a gentle-beam mode) without a metal coating. High-resolution TEM images were taken by using a Tecnai G2 F30 with an accelerating voltage of 300 kV. The specific surface area, pore volume and pore size distribution were analyzed with N_2 adsorption-desorption isotherms, which were measured at 77 K with a Micromeritics Tristar II volumetric adsorption analyzer. Prior to the adsorption measurements, all samples were degassed under a vacuum for 12 h at 573 K. The surface area was calculated from the adsorption branch in the P/P_0 range between 0.05 and 0.20 using the Brunauer−Emmett−Teller (BET) equation. The pore size distributions were converted from the entire adsorption branch according to the Barrett−Joyner−Halenda (BJH) algorithm for approximation.[27]

dx.doi.org/10.1021/cm201709q | *Chem. Mater.* 2011, 23, 5131−5137

Table 2. Zeolite Synthesis Conditions

	gel composition in mole ratios							
SDA	SDA	SiO_2	Na_2O	H_2SO_4	H_2O	EtOH	silica source	reaction time (d)
$C_{22-i}N_2Br_2$	10	100	30	18	4000	0	water glass	4
$C_{22}N_1Br$	10	100	30	18	4000	400	TEOS	4
$C_{22-6}N_n(OH)_n$	2.5−5	100	0	0	4000	400	TEOS	9
$C_{18-6}N_2(R_2)Br_2$	10	100	30	18	4000	0 or 400	water glass	5
$C_{18-6}N_2(Pr_3)Br_2$	10	100	30	18	4000	0	water glass	5
$C_{m-6}N_2Br_2$	10	100	30	18	4000	400	TEOS	4

RESULTS AND DISCUSSION

Effective Length of Alkylene Spacer between Ammoniums. The synthesis of zeolite with $C_{22-i}N_2$ [i.e., $C_{22}H_{45}-N^+(CH_3)_2-C_iH_{2i}-N^+(CH_3)_2-C_6H_{13}$, i = 3, 6, 8] was performed at the gel composition of 100 SiO_2: 10 $C_{22-i}N_2$: 30 Na_2O: 18 H_2SO_4: 4000 H_2O in mole ratios as given in Table 2. The surfactants were used in the bromide form. Water glass was used as a silica source. Figure 1 shows the powder XRD patterns of the zeolite products before calcination. All the XRD patterns indicated MFI structure, but there were remarkable differences among SDAs. When the SDA was $C_{22-6}N_2$, the small-angle diffraction pattern showed two Bragg diffractions at 2θ = 1.35° (d = 6.5 nm) and 4.05° (d = 2.2 nm) [Figure 1A(a)]. This result indicated that the product was a layered material with the interlayer spacing of 4.5 nm. (The interlayer spacing is variable depending on washing and drying conditions, which can extract more or less the "dummy filler" surfactant molecules.[24]) The product exhibited Bragg diffraction lines in the wide-angle diffraction pattern, which could be assigned to an MFI-type zeolite, except for the reflections corresponding to structural order in the direction of b-axis [Figure 1B(a)]. From this result, it was concluded that the $C_{22-6}N_2$ surfactant generated a multilamellar structure composed of extremely thin MFI.[24,25] When $C_{22-8}N_2$ was used as the SDA, the wide-angle XRD pattern in Figure 1B(b) was very similar to the result from $C_{22-6}N_2$. However, the small-angle peaks disappeared [Figure 1A(b)]. This indicated that the zeolite from $C_{22-8}N_2$ was an irregular assembly of nanosheets (i.e., *unilamellar* zeolite).[24,26] The zeolite after calcination exhibited high specific BET surface area (590 m^2 g^{-1}) and total pore volume (0.7 cm^3 g^{-1}), compared with the multilamellar zeolite product (510 m^2 g^{-1} and 0.4 cm^3 g^{-1}) obtained from $C_{22-6}N_2$. On the other hand, when $C_{22-3}N_2$ was used, the XRD pattern indicated that the product was not nanosheets but a bulk MFI zeolite [Figure 1B(c)]. All the wide-angle XRD reflections were very narrow lines that were indexable to the bulk zeolite. The small-angle diffractions were totally missing [Figure 1A(c)].

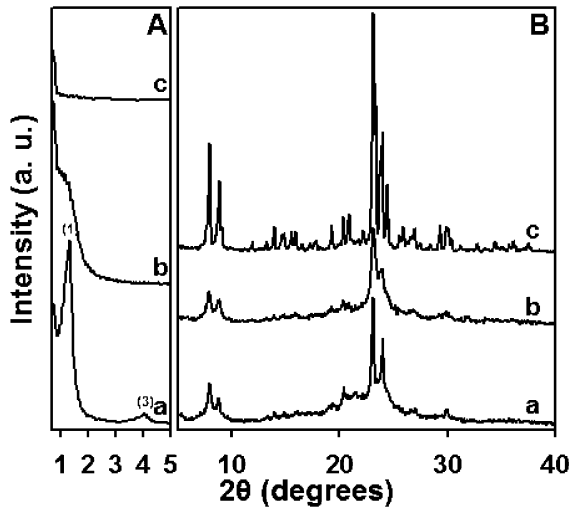

Figure 1. Small-angle (A) and wide-angle (B) powder XRD patterns for as-synthesized products, which were obtained with (a) $C_{22-6}N_2Br_2$, (b) $C_{22-8}N_2Br_2$, and (c) $C_{22-3}N_2Br_2$ surfactants.

The structural information from the XRD patterns was in good agreement with high-resolution SEM and TEM images (Figure 2). The zeolite product from $C_{22-6}N_2$ was identical to the multilamellar MFI nanosheets reported by Choi et al. [Figures 2(A, B)], in which 2 nm thick zeolite nanosheets were equally spaced by a 3 nm layer of surfactant tails. In the case of $C_{22-8}N_2$ [Figures 2(C, D)], the zeolite nanosheets were relatively narrow and irregularly assembled.[26] When $C_{22-3}N_2$ was used, as shown by the SEM and TEM images [Figures 2(E, F)], the resultant zeolite product was micrometer-sized bulk crystals. The crystal morphologies were very similar to a bulk

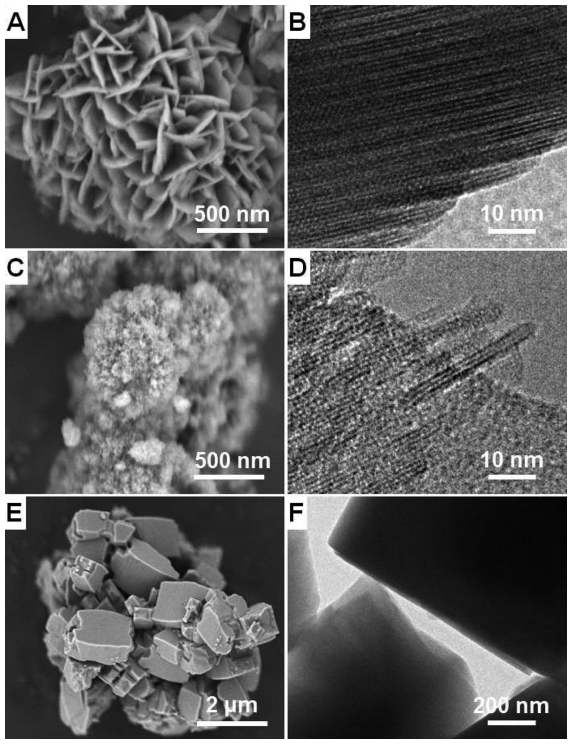

Figure 2. High-resolution SEM (left column) and TEM (right column) images of as-synthesized products, which were obtained with (A, B) $C_{22-6}N_2Br_2$, (C, D) $C_{22-8}N_2Br_2$, and (E, F) $C_{22-3}N_2Br_2$ surfactants.

dx.doi.org/10.1021/cm201709q | Chem. Mater. 2011, 23, 5131–5137

MFI zeolite that could normally be synthesized with TPA^+. The color of the synthesis mixture changed from white to dark brown during the hydrothermal reaction. A very unpleasant odor was generated after the hydrothermal reaction for 4 d at 140 °C. This change indicated that the $C_{22-3}N_2$ surfactant was likely to decompose to small amine molecules via Hofmann elimination under the basic condition at high temperature. The resultant small organic amine seemed to act as a bulk zeolite SDA. The instability of $C_{22-3}N_2$ could be due to the short $-C_3H_6-$ spacer, which was insufficient to separate the charges between the two ammonium cations. In comparison, the $C_{22-6}N_2$ and $C_{22-8}N_2$ surfactants with $-C_6H_{12}-$ and $-C_8H_{16}-$ spacers were sufficiently stable although there was a slight difference in the product morphologies. The $C_{22-6}N_2$ surfactant could organize the multilamellar mesostructure while $C_{22-8}N_2$ led to the generation of disordered nanosheets. This difference may be explained with different packing parameters.

To investigate why the $-C_6H_{12}-$ and $-C_8H_{16}-$ spacers cause different registration of the MFI layers, computer simulations were carried out. In this preliminary study, the diquaternary ammonium molecules of the formula with $(C_3H_7)_3N^+-C_iH_{2i}-N^+(C_3H_7)_3$, where i = 6 and 8, were used as a simplified model of the $C_{22-6}N_2$ organic surfactants. The potential packing arrangements of the two organic templates were explored within fully periodic MFI. Using a force field approach, which has been successfully used previously,[28,29] a single template with i = 6 or i = 8 was geometry optimized within a 1 × 2 × 1 supercell of MFI (see Supporting Information for the computation details). The template with i = 6 was found to bind more strongly than i = 8 within the straight [010] channel lattice by just 15 kJ mol^{-1}, suggesting that both templates have similar stabilizing effect on the bulk lattice. The adsorption of the template with i = 6 in the sinusoidal channel [100] was less favorable than that in the straight channel by more than 80 kJ mol^{-1}, indicating an extremely strong preference for location in the [010] channel. In the case of i = 8, no minimum energy structure was found for the [100] channel, which also suggests preferential adsorption on the [010] channel. In the Supporting Information, we show the optimized arrangement of the templates in the [010] channel i = 6 and i = 8 (Supporting Information, Figure S1 for i = 6, and Supporting Information, Figure S2 for i = 8). In the case of i = 6, the N^+ center lies below a plane containing oxygen atoms, while for i = 8, the N^+ center lies above this plane. This may be significant because the plane of oxygen atoms is equivalent to that exposed on the 3-pentasil-layer slab, where the oxygen atoms are terminal silanol groups. For the i = 6 template within the slab, the negatively charged hydroxyl groups envelop the positively charged N^+ center, presumably anchoring the N^+ center. Because the N^+ center in the case of i = 8 lies above the terminal silanols, the C_{22} tail will presumably be more mobile, preventing interdigitation of the C_{22} tails, leading to unilamellar MFI.

In our previous work,[24] it was assumed that there were two templates per 96 T sites in the 3-pentasil-layer MFI slab. However, in either case of $C_{22-6}N_2$ or $C_{22-8}N_2$, two templating molecules cannot occupy the same channel because of steric repulsion. Since the zeolite templates must occupy the neighboring channels to meet the experimentally determined template density per unit cell, the remaining question is what the positioning of the second template relative to the first one would be. According to simulation, the optimal positioning of the template is achieved when the distance between templates is maximized, which is driven by the need to minimize the electrostatic repulsion between the two positively charged templates. Hence, a similarly ordered arrangement of templates for i = 6 and i = 8 is predicted, as depicted in Supporting Information, Figure S3.

Increase in Nanosheet Thickness by Ammonium Number. Figure 3 shows the XRD patterns for the as-synthesized silica products (before calcinations), which were synthesized with $C_{22-6}N_n$ surfactants. As described in Table 1, n was varied from 2 to 4, and the ratio of SiO_2 per N^+ in the surfactant was fixed to 10 in the gel composition. Here, the synthesis was performed under a Na^+-free condition by using the hydroxide form of the surfactants, to exclude the possibility for the zeolite generation by Na^+. As the XRD patterns and TEM images show, all the zeolite products were in the form of nanosheets (Figures 3, 4). When $C_{22-6}N_2$ was used as the SDA, every nanosheet was composed of exactly 3-pentasil layers to the same thickness of 2 nm (Figure 4A). The nanosheets self-assembled into a multilamellar structure as in the product discussed above. When the higher oligomeric ammonium compounds, $C_{22-6}N_3$ and $C_{22-6}N_4$, were used, the nanosheet thickness increased progressively with the number of ammonium groups in a molecule. The structural coherence between nanosheets was lost [Figures 3A(b, c)], probably because of the increasing thickness. In the case of the $C_{22-6}N_3$ molecule, most of the nanosheets were composed of 5-pentasil layers. As seen in Figure 4B, there are images appearing much thicker than the 5-pentasil nanosheets. But they seem to be due to overlap of two or more nanosheets. In the case of $C_{22-6}N_4$, the nanosheet thickness increased to 7 or sometimes more pentasil layers (Figure 4C). Compared with the formation of zeolite nanosheets by $C_{22-6}N_2$, $C_{22-6}N_3$, and $C_{22-6}N_4$, the synthesis attempt using $C_{22}N_1$ [i.e., $C_{22}H_{45}-N^+(CH_3)_2-C_6H_{13}$] was never successful to generate a zeolite framework (Figures 3, 4). The product was a non-porous, layered silicate phase like the hexadecyltrimethyl ammonium surfactant in previous studies.[30,31]

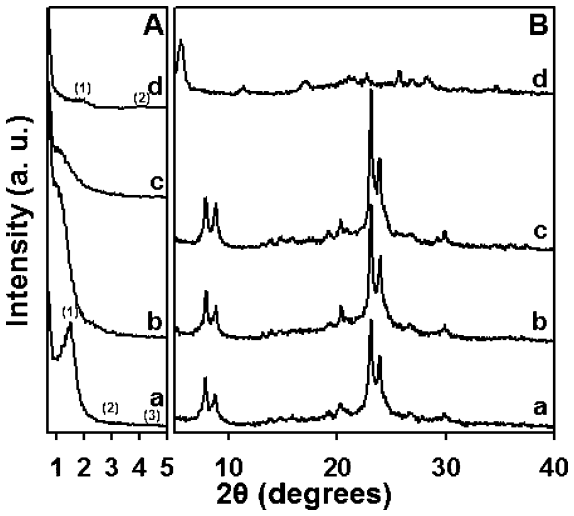

Figure 3. Small-angle (A) and wide-angle (B) powder XRD patterns for as-synthesized products, which were obtained with (a) $C_{22-6}N_2(OH)_2$, (b) $C_{22-6}N_3(OH)_3$, (c) $C_{22-6}N_4(OH)_4$, and (d) $C_{22}N_1Br$ surfactants, under the same SiO_2/N^+ ratio at 10 in the gel compositions.

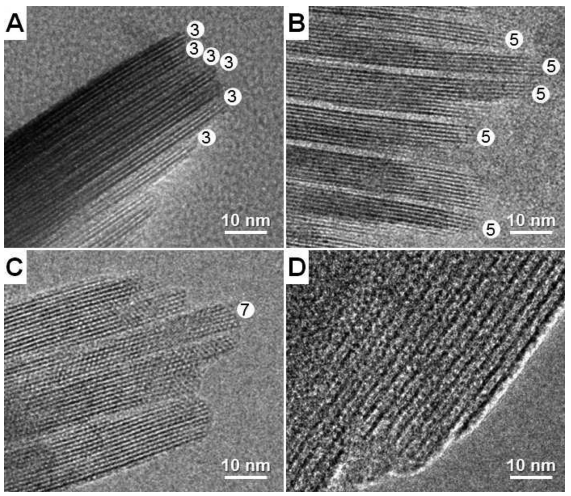

Figure 4. High-resolution TEM images for as-synthesized products, which were obtained with (a) $C_{22-6}N_2(OH)_2$, (b) $C_{22-6}N_3(OH)_3$, (c) $C_{22-6}N_4(OH)_4$, and (d) $C_{22}N_1Br$ surfactants. The value in white circles indicates the number of pentasil sheets in a nanosheet.

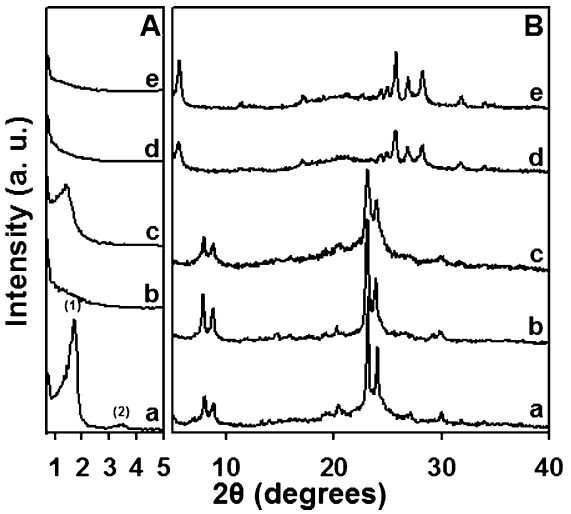

Figure 5. Small-angle (A) and wide-angle (B) powder XRD patterns for as-synthesized products, which were obtained with (a) $C_{18-6}N_2(Me_2)Br_2$, (b) $C_{18-6}N_2(Et_2)Br_2$, (c) $C_{18-6}N_2(Pr_3)Br_2$, (d) $C_{18-6}N_2(Pr_2)Br_2$, and (e) $C_{18-6}N_2(Bu_2)Br_2$ surfactants.

Evidently, one ammonium is not enough for the formation of the microporous zeolitic framework. At least two ammoniums are necessary for directing the zeolite structure. The ammonium group directly bonded to the C_{22}-alkyl tail looks like a hinge joining other ammonium groups to promote the zeolite structure-directing function. Here, the role of the $C_{22-6}N_n$ surfactant is two-fold. The multi-ammonium head acts as a zeolite SDA while the surfactant tails intermolecularly self-assemble into the lamellar-type mesostructure because of the hydrophobic interaction. The nanosheet thickness can be increased more preferably along the *b*-axis than other axes by the number of ammonium groups although uniformity is somewhat decreased. Such preferred crystal growth is due to the favorable orientation of multi-ammonium headgroup within the straight channel along the *b*-axis, which is consistent with the previous reports on the synthesis of MFI zeolites with organic polycations.[32−34]

Alkyl Moieties in the Terminal Ammonium. The effect of the alkyl groups at the terminal ammonium was also investigated. Figure 5 shows the XRD patterns of the as-synthesized products, which were synthesized with the $C_{18-6}N_2(R)$ surfactants (where, R = Me_2, Et_2, Pr_2, Bu_2, and Pr_3) as described in Table 1. The XRD results in Figure 5 indicate that the alkyl groups were an important factor affecting the zeolite crystallization. When the alkyl groups were Me_2, Et_2, and Pr_3, the MFI zeolite nanosheets were generated [Figures 5B(a−c)]. However, in the case of $C_{18-6}N_2(Pr_2)$ and $C_{18-6}N_2(Bu_2)$, an unknown silicate phase without specific mesostructural order was generated [Figures 5B(d, e)]. The silicate structure completely collapsed upon high-temperature calcination.

As already reported in many reports, zeolite frameworks can be formed via the single-molecular templating mechanism by organic ammonium molecules that are co-operatively assembled with anionic silicate species.[1,2,4,5] Such organic SDA-mediated crystallization process is well-known to be affected by the size, charge, hydrophilicity (C/N^+ ratio), and shape of the organic SDA.[35,36] Similarly, in the present surfactant-mediated synthesis of nanosheet zeolite, the size and hydrophilicity according to the C/N^+ ratio of the terminal ammonium can play a crucial role on the direction of zeolite framework. In the series of $C_{18-6}N_2(Me_2)$, $C_{18-6}N_2(Et_2)$, $C_{18-6}N_2(Pr_3)$, $C_{18-6}N_2(Pr_2)$, and $C_{18-6}N_2(Bu_2)$, the kinetic size and C/N^+ ratio of the terminal ammonium region progressively increased in concert with the decrease in the hydrophilicity. As the volume of the terminal ammonium increases, the templating function for MFI zeolite is progressively lost because of the mismatch between the size of organic ammonium and zeolite micropore. At the same time, the hydrophobicity can increase to beyond the solubility or hydration range. This will prevent the contact between the ammonium group and the silicate anion, hindering the structure-directing function.

Length of Surfactant Tail. For the formation of MFI nanosheet, the surfactant tail should have sufficient hydrophobic interaction between the tails in neighboring molecules to self-assemble into a specific micellar structure (i.e., lamellar mesostructure in the present case). The tails should form a bulky hydrophobic barrier in the micelle, so that the zeolite structure generation is confined within the headgroup region. If these conditions are satisfied, the nanosheet thickness can be controlled according to the ammonium number. In this section, we examine the detailed effects of the hydrophobic tail length on the morphologies of the resultant zeolite as the C_{22}-alkyl chain in $C_{22-6}N_2$ is replaced by C_{12}, C_{10}, C_8, and C_6.

The XRD patterns in Figure 6 were obtained from the synthesized products (before calcinations) using the C_{12}−C_6 compounds. As judged by these XRD patterns, all the products were fully crystalline MFI zeolites (Figure 6B), irrespective of the alkyl tail lengths. In particular, in the range of C_{12}−C_{10}, the zeolite was generated with the multilamellar nanosheet-type mesostructure [Figures 7(A, B)]. The small-angle XRD patterns show the first and second reflections corresponding to the multilamellar structure [Figures 6A(a, b)]. The wide-angle XRD reflections along *b*-axis were missing, implying that the nanosheet crystals with wide *a*-*c* plane were formed [Figures 6B(a, b)]. The thickness of these nanosheets was 2 nm. On the other hand, as the tail length decreased to C_8 or C_6, the zeolite morphology changed to 3-dimensional crystals [Figures 7(C, D)]. The zeolite products from $C_{8-6}N_2$ and $C_{6-6}N_2$ diquaternary ammoniums exhibited all the (*hkl*) reflections of the 3-dimensional MFI framework. No specific

dx.doi.org/10.1021/cm201709q|*Chem. Mater.* 2011, 23, 5131−5137

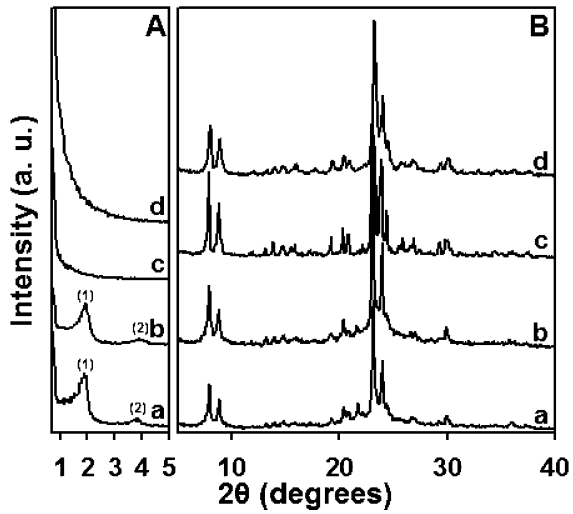

Figure 6. Small-angle (A) and wide-angle (B) powder XRD patterns for as-synthesized products, which were obtained with (a) $C_{12-6}N_2Br_2$, (b) $C_{10-6}N_2Br_2$, (c) $C_{8-6}N_2Br_2$, and (d) $C_{6-6}N_2Br_2$ diquaternary ammoniums.

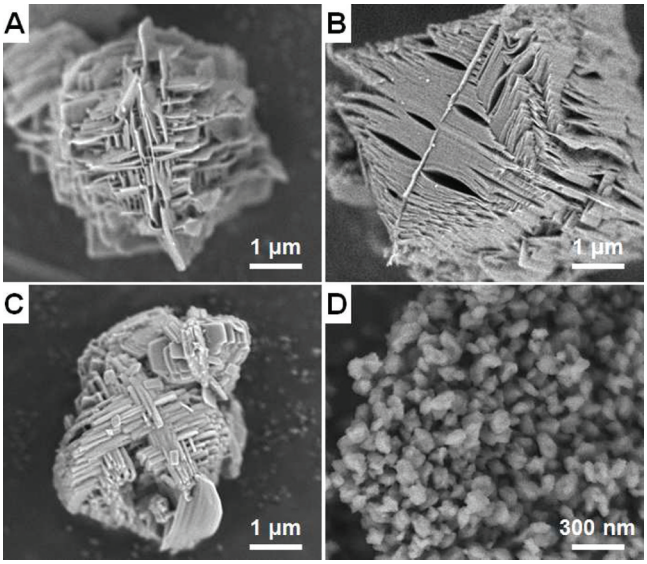

Figure 7. High-resolution SEM images of as-synthesized products, which were obtained with (A) $C_{12-6}N_2Br_2$, (B) $C_{10-6}N_2Br_2$, (C) $C_{8-6}N_2Br_2$, and (D) $C_{6-6}N_2Br_2$ diquaternary ammoniums.

ordered mesostructures were detected in the small-angle XRD region. Although the zeolite product from $C_{8-6}N_2$ exhibited plate-like shape, the thickness was much more than 2 nm, as shown in the TEM image in Supporting Information, Figure S4(C). The morphologies indicate that the zeolite crystals continue to grow in 3 dimensions. This type of zeolite growth occurs typically by incorporating SDA molecules, without termination by the alkyl tails. In the case of $C_{6-6}N_2$, the zeolite crystal growth also occurred in a 3-dimensional manner. However, the crystals were tiny nanoparticles about the size of 100−150 nm (Figure 7D).

CONCLUSION

We investigated the hierarchically structure-directing effect of multi-quaternary ammonium surfactants for the generation of MFI zeolite nanosheets, modifying the detailed surfactant structures such as the N−N spacer length, number of ammonium groups, alkyl groups in ammonium, and hydrophobic tail length. Our results provided the following information: first, there was an optimum spacer length (i.e., $-C_iH_{2i}-$) in the case of the nanosheet formation by $C_{22}H_{45}-N^+(CH_3)_2-C_iH_{2i}-N^+(CH_3)_2-C_6H_{13}$. When i = 3, the surfactant was decomposed to small molecules via Hofmann elimination. The resultant small amine molecules generated bulk MFI crystals. When i = 6 or 8, the zeolite nanosheets were obtained. The nanosheets were arranged in an ordered multilamellar manner when i = 6, under the present synthesis condition. When i = 8, the nanosheets were assembled in a disordered manner, self-retaining a large volume of mesopores. Modeling suggests that for i = 8, the C_{22} group is likely to be more mobile and this would hinder ordered interdigitation of lamellae. Second, at least two ammonium groups were required for the formation of the zeolite nanosheets. The first ammonium group, which was bonded directly to the surfactant tail, did not seem to function as a template for the zeolite structure. The thickness of the nanosheets could be progressively increased according to the number of ammonium groups except the one bonded directly to the surfactant tail. Third, the size of the structure-directing moiety should fit well for the MFI micropore generation. The C/N^+ ratio at the terminal ammonium should be also optimized. That is, the surfactants having alkyl moiety with bulky structure and high C/N^+ ratio failed to generate the zeolite. Finally, the surfactant tail (i.e., C_mH_{2m+1}) should be sufficiently long (m = 10−22) to self-assemble into a specific micellar structure and thereby to confine the crystal growth within the ammonium region. When the tail was too short ($m \leq 8$), the SDA molecules were fully embedded inside MFI micropores without stopping the zeolite crystal growth. The structural effects of the surfactant provided here would be helpful for designing other surfactant molecules for the synthesis of other nanomorphic zeolites in the future.

ASSOCIATED CONTENT

Supporting Information

Detailed synthesis procedures of the quaternary ammonium surfactants, SEM, TEM, and computational analyses. This material is available free of charge via the Internet at http://pubs.acs.org.

AUTHOR INFORMATION

Corresponding Author

*E-mail: rryoo@kaist.ac.kr.

ACKNOWLEDGMENTS

This work was supported by the National Honor Scientist Program (20100029665) and World Class University Program (R31-2010-000-10071-0) of the Ministry of Education, Science and Technology in Korea. Y.S. acknowledges support from SCF (Special Coordination Funds for Promoting Science and Technology) by MEXT of Japan. B.S. would like to thank Mr. Tony Xiao for preliminary work on this topic.

REFERENCES

(1) Cundy, C. S.; Cox, P. A. *Chem. Rev.* **2003**, *103*, 663.
(2) Corma, A. *Chem. Rev.* **1997**, *97*, 2373.
(3) Corma, A. *J. Catal.* **2003**, *216*, 298.
(4) Davis, M. E.; Lobo, R. F. *Chem. Mater.* **1992**, *4*, 756.
(5) Corma, A.; Davis, M. E. *ChemPhysChem* **2004**, *5*, 304.

(6) Egeblad, K.; Christensen, C. H.; Kustova., M.; Christensen, C. H. *Chem. Mater.* **2008**, *20*, 946.
(7) Pérez-Ramírez, J.; Christensen, C. H.; Egeblad, K.; Christensen, C. H.; Groen, J. C. *Chem. Soc. Rev.* **2008**, *37*, 2530.
(8) Davis, M. E. *Nature* **2002**, *417*, 813.
(9) Kresge, C. T.; Leonowicz, M. E.; Roth, W. J.; Vartuli, J. C.; Beck, J. S. *Nature* **1992**, *359*, 710.
(10) Zhao, D.; Feng, J.; Huo, Q.; Melosh, N.; Frederickson, G. H.; Chmelka, B. F.; Stucky, G. D. *Science* **1998**, *279*, 548.
(11) Cassiers, K.; Linssen, T.; Mathieu, M.; Benjelloun, M.; Schrijnemakers, K.; Van Der Voort, P.; Cool, P.; Vansant, E. F. *Chem. Mater.* **2002**, *14*, 2317.
(12) Zhao, D.; Nie, C.; Zhou, Y.; Xia, S.; Huang, L.; Li, Q. *Catal. Today* **2001**, *68*, 11.
(13) Srivastava, R.; Choi, M.; Ryoo, R. *Chem. Commun.* **2006**, 4489.
(14) Shetti, V. N.; Kim, J.; Srivastava, R.; Choi, M.; Ryoo, R. *J. Catal.* **2008**, *254*, 296.
(15) Kim, J.; Choi, M.; Ryoo, R. *J. Catal.* **2010**, *269*, 219.
(16) Tosheva, L.; Valtchev, V. P. *Chem. Mater.* **2005**, *17*, 2494.
(17) Müller, M.; Harvey, G.; Prins, R. *Microporous Mesoporous Mater.* **2000**, *34*, 135.
(18) Groen, J. C.; Bach, T.; Ziese, U.; Donk, A. M. P.; de Jong, K. P.; Moulijn, J. A.; Pérez-Ramírez, J. *J. Am. Chem. Soc.* **2005**, *127*, 10792.
(19) Groen, J. C.; Moulijn, J. A.; Pérez-Ramírez, J. *J. Mater. Chem.* **2006**, *16*, 2121.
(20) Jacobsen, C. J. H.; Madsen, C.; Houzvicka, J.; Schmidt, I.; Carlsson, A. *J. Am. Chem. Soc.* **2000**, *122*, 7116.
(21) Schmidt, I.; Boisen, A.; Gustavsson, E.; Ståhl, K.; Pehrson, S.; Dahl, S.; Carlsson, A.; Jacobsen, C. J. H. *Chem. Mater.* **2001**, *13*, 4416.
(22) Yang, Z.; Xia, Y.; Mokaya, R. *Adv. Mater.* **2004**, *16*, 727.
(23) Choi, M.; Cho, H. S.; Srivastava, R.; Venkatesan, C.; Choi, D.-H.; Ryoo, R. *Nat. Mater.* **2006**, *5*, 718.
(24) Choi, M.; Na, K.; Kim, J.; Sakamoto, Y.; Terasaki, O.; Ryoo, R. *Nature* **2009**, *461*, 246.
(25) Na, K.; Choi, M.; Park, W.; Sakamoto, Y.; Terasaki, O.; Ryoo, R. *J. Am. Chem. Soc.* **2010**, *132*, 4169.
(26) Na, K.; Park, W.; Seo, Y.; Ryoo, R. *Chem. Mater.* **2011**, *23*, 1273.
(27) Ravikovitch, P. I.; Domhnaill, S. C. O.; Neimark, A. V.; Schueth, F.; Unger, K. K. *Langmuir* **1995**, *11*, 4765.
(28) Whitmore, L.; Slater, B.; Catlow, C. R. A. *Phys. Chem. Chem. Phys.* **2000**, *2*, 5354.
(29) Chiu, M. E.; Slater, B.; Gale, J. D. *Angew. Chem. Int. Ed.* **2005**, *44*, 1213.
(30) Huo, Q.; Margolese, D. I.; Stucky, G. D. *Chem. Mater.* **1996**, *8*, 1147.
(31) Hedin, N.; Graf, R.; Christiansen, S. C.; Gervais, C.; Hayward, R. C.; Eckert, J.; Chmelka, B. F. *J. Am. Chem. Soc.* **2004**, *126*, 9425.
(32) de Vos Burchart, E.; Jansen, J. C.; van de Graaf, B.; van Bekkum, H. *Zeolites* **1993**, *13*, 216.
(33) Lai, Z.; Bonilla, G.; Díaz, I.; Nery, J. G.; Sujaoti, K.; Amat, M. A.; Kokkoli, E.; Terasaki, O.; Thompson, R. W.; Tsapatsis, M.; Vlachos, D. G. *Science* **2003**, *300*, 456.
(34) Bonilla, G.; Díaz, I.; Tsapatsis, M.; Jeong, H.-K.; Lee, Y.; Vlachos, D. G. *Chem. Mater.* **2004**, *16*, 5697.
(35) Kubota, Y.; Helmkamp, M. M.; Zones, S. I.; Davis, M. E. *Microporous Mater.* **1996**, *6*, 213.
(36) Goretsky, A. V.; Beck, L. W.; Zones, S. I.; Davis, M. E. *Microporous Mesoporous Mater.* **1999**, *28*, 387.